Experimental quantum entanglement and teleportation by tuning remote spatial indistinguishability of independent photons

KAI SUN[1,2], YAN WANG[1,2], ZHENG-HAO LIU[1,2], XIAO-YE XU[1,2], JIN-SHI XU[1,2,*], CHUAN-FENG LI[1,2,**], GUANG-CAN GUO[1,2], ALESSIA CASTELLINI[3], FARZAM NOSRATI[4,5], GIUSEPPE COMPAGNO[3], AND ROSARIO LO FRANCO[3,6,§]

[1] CAS Key Laboratory of Quantum Information, University of Science and Technology of China, Hefei 230026, China
[2] Synergetic Innovation Center of Quantum Information and Quantum Physics, University of Science and Technology of China, Hefei 230026, China
[3] Dipartimento di Fisica e Chimica - Emilio Segrè, Università di Palermo, via Archirafi 36, 90123 Palermo, Italy
[4] Dipartimento di Ingegneria, Università di Palermo, Viale delle Scienze, Edificio 9, 90128 Palermo, Italy
[5] INRS-EMT, 1650 Boulevard Lionel-Boulet, Varennes, Québec J3X 1S2, Canada
[6] Dipartimento di Ingegneria, Università di Palermo, Viale delle Scienze, Edificio 6, 90128 Palermo, Italy
[*] Corresponding author: jsxu@ustc.edu.cn
[**] Corresponding author: cfli@ustc.edu.cn
[§] Corresponding author: rosario.lofranco@unipa.it

Compiled October 26, 2020

Quantitative control of spatial indistinguishability of identical subsystems as a direct quantum resource at distant sites has not been yet experimentally proven. We design a setup capable to tune remote spatial indistinguishability of two independent photons by individually adjusting their spatial distribution in two distant regions, leading to polarization entanglement from uncorrelated photons. This is achieved by spatially localized operations and classical communication (sLOCC) on photons which only meet at the detectors. The amount of entanglement uniquely depends on the degree of spatial indistinguishability, quantified by an entropic measure $\mathcal{I}$, which enables teleportation with fidelities above the classical threshold. The results open the way to viable indistinguishability-enhanced quantum information processing.

http://dx.doi.org/10.1364/ao.XX.XXXXXX

Discovering how fundamental traits of quantum constituents can facilitate preparation and control of composite systems is strategic for the scientific progress. In fact, this achievement impacts both on the advance of our knowledge of the basic features of the natural world and on the development of quantum-enhanced technologies. Many-body quantum networks are usually made of identical building blocks, such as atoms, electrons, photons or generic qubits [1–5]. Indistinguishability of identical subsystems thus emerges as inherent quantum feature that may play a role in quantum information processing.

The usual request to implement quantum tasks in many-body systems is that qubits are individually addressed, which have been experimentally realized with various apparatuses [6]. For nonidentical qubits, this requirement is fulfilled by local operations and classical communication (LOCC), where the term "local" refers to particle-locality independently of their spatial configuration [6]. Differently, identical qubits are not in general individually addressable [7], spatial distribution of their wave functions becoming crucial. Despite the long debate about formal aspects on entanglement of identical particles [7–20] and some proposals using particle identity for quantum protocols [5, 21–25], experimental evidence of spatial indistinguishability as a direct resource has remained elusive, because of the lack of its proper informational measure and a suitable control technique.

Here we experimentally implement the operational framework based on spatially localized operations and classical communication (sLOCC) which, at variance with the idea of particle locality, relies on the concept of spacial locality of measurement as in quantum field theory [24]. The setup is capable to control the distribution of the wave packets of two independent initially-uncorrelated identical photons towards two separated (remote) operational regions where the photons are collected. This allows for continuously adjusting the degree of their remote spatial indistinguishability, quantified via a suitable entropic-informational measure [26]. The two photon paths remain separated along the setup and only meet in the operational regions. By single-photon localized measurements, we prove that the two uncorrelated photons with opposite polarizations get entangled, the amount of entanglement being only related to the degree of spatial indistinguishability. We show that the nonlocal entanglement so generated violates the Bell inequality and activates conditional teleportation of the state of an additional photon with fidelities higher than the classical threshold.

Theory. We start describing the basic theoretical setup, depicted in Fig. 1A. Two identical particles, coming from independent sources, are in the initial uncorrelated state $|\psi\uparrow,\psi'\downarrow\rangle$,

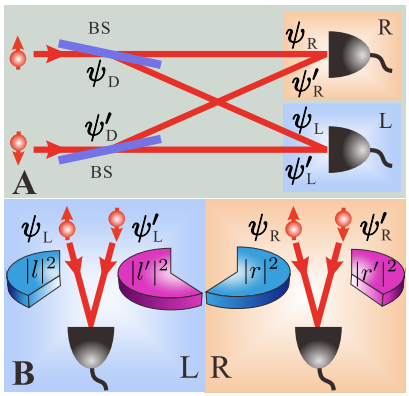

Fig. 1. (A) Theoretical setup. (B) Generic spatial distribution of particles in the state $|\Psi\rangle = |\psi_D \uparrow, \psi'_D \downarrow\rangle$, with $|\psi_D\rangle = l\,|\psi_L\rangle + r\,|\psi_R\rangle$ and $|\psi'_D\rangle = l'\,|\psi'_L\rangle + r'\,|\psi'_R\rangle$ $(0 < \mathcal{I} < 1)$.

written in the no-label formalism [17] (see section A in Supplementary Material (SM)). Each particle wave packet is then distributed in a controllable manner towards two remote operational regions L and R by a beam splitter (BS), $|\psi\rangle \xrightarrow{\text{BS}} |\psi_D\rangle$ and $|\psi'\rangle \xrightarrow{\text{BS}} |\psi'_D\rangle$. The sLOCC measurements, represented by the two detectors in Fig. 1A, are realized by localized single-particle counting in each region (sLO) and coincidence measures (CC). Taking photons as identical particles, this scheme can be seen as a modified Hanbury Brown and Twiss experiment [27, 28], the modification consisting in initially polarizing the photons and in controlling their spatial distribution. Before sLOCC, the two-particle state is $|\Psi\rangle = |\psi_D \uparrow, \psi'_D \downarrow\rangle$, where $|\psi_D\rangle = l\,|\psi_L\rangle + r\,|\psi_R\rangle$ $(|l|^2 + |r|^2 = 1)$ and $|\psi'_D\rangle = l'\,|\psi'_L\rangle + r'\,|\psi'_R\rangle$ $(|l'|^2 + |r'|^2 = 1)$, with $|\psi_X\rangle$, $|\psi'_X\rangle$ (X = L, R) indicating the two wave packets located in the operational region X. Particle paths do not share any common past and meet only at the detection level, so that to the eyes of the localized measurement devices the particles are indistinguishable and individually unaddressable. The question arises whether $|\Psi\rangle$ contains useful pseudospin entanglement in L and R, a longly debated conceptual issue [24]. Particle spatial overlap occurs at distant sites, defining a remote spatial indistinguishability quantified by the entropic measure [26]

$$\mathcal{I} = -\sum_{i=1}^{2} p_{\text{LR}}^{(i)} \log_2 p_{\text{LR}}^{(i)}, \qquad \textbf{(1)}$$

where $p_{\text{LR}}^{(1)} = |lr'|^2/(|lr'|^2 + |l'r|^2)$ and $p_{\text{LR}}^{(2)} = 1 - p_{\text{LR}}^{(1)}$ (see section A in SM for details). Here $|lr'|^2$ is the joint probability of finding a particle in L coming from $|\psi_D\rangle$ and a particle in R coming from $|\psi'_D\rangle$, whilst $|l'r|^2$ is clearly the vice versa (see Fig. 1B). This measure ranges from $\mathcal{I} = 0$ for separated wave packets ($|l|^2 = |r'|^2 = 1$ or $|l|^2 = |r'|^2 = 0$) to $\mathcal{I} = 1$ for equally distributed wave packets ($|l|^2 = |l'|^2$) (see section B in SM). Any other particle degree of freedom, apart spatial location, has no effect on $\mathcal{I}$. Applying the projector $\hat{\Pi}_{\text{LR}} = \sum_{\sigma,\tau=\uparrow,\downarrow} |\text{L}\sigma, \text{R}\tau\rangle\langle \text{L}\sigma, \text{R}\tau|$, which defines localized single-particle counting in L and R, on $|\Psi\rangle$ gives [24]

$$|\Psi_{\text{LR}}\rangle = (lr'|\text{L}\uparrow, \text{R}\downarrow\rangle + \eta rl'|\text{L}\downarrow, \text{R}\uparrow\rangle)/(\sqrt{|lr'|^2 + |rl'|^2}), \qquad \textbf{(2)}$$

with probability $P_{\text{LR}} = |lr'|^2 + |rl'|^2$, where $\eta = \pm 1$ for bosons and fermions, respectively.

Experiment. The experimental setup realizing this theoretical scheme is displayed in Fig. 2A. Two (uncorrelated) heralded single photons are emitted independently via spontaneous parametric down conversion (SPDC) from two BBO crystals, designed to satisfy beamlike type-II SPDC [29] and pumped by pulsed ultraviolet light at 400 nm. The two photons (of wavelength 800 nm) are initially polarized in $|H\rangle$ (horizontal, $H \equiv \uparrow$) and $|V\rangle$ (vertical, $V \equiv \downarrow$) polarization, respectively, and then collected separately by two single-mode fibers via fiber couplers (FCs). At this stage, the photons are completely uncorrelated in the state $|H\rangle \otimes |V\rangle$, as verified with high fidelity $(95.2 \pm 0.7)\%$ (see section C in SM). Before the main experiment, we perform usual two-photon interference to reveal the identity of the employed operational photons characterized by visibility of Hong-Ou-Mandel (HOM) dip [30], giving a value of $\approx 83.8\%$ (see section C in SM). The BSs of Fig. 1A are actually substituted by the sequence of a half-wave plate (HWPi, $i = 1, 2$), a polarizing beam-splitter (PBS) and two final HWPs at 45° before the location L. By rotating HWP1 and HWP2 at angles $(\pi/2 - \alpha)/2$ and $-\beta/2$, respectively, we can conveniently adjust the weights of the linear spatial distribution of the photons on the two measurement sites, while the PBSs separate the different polarizations. The final HWPs at 45° are needed to maintain the initial polarization of each photon unvaried. In each region L and R a beam displacer (BD) makes the paths of the two photons meet at the detection level. It is straightforward to see that this setup prepares the desired state $|\Psi_{\text{prep}}\rangle = |\psi_D H, \psi'_D V\rangle$ with $|\psi_D\rangle = \cos\alpha\,|\psi_L\rangle + \sin\alpha\,|\psi_R\rangle$ and $|\psi'_D\rangle = \sin\beta\,|\psi'_L\rangle + \cos\beta\,|\psi'_R\rangle$. By setting α and β, we can prepare a series of $|\Psi_{\text{prep}}\rangle$ for different spatial distributions and thus for various values of $\mathcal{I}$. All the optical elements of the setup independently act on each photon, so the photon states $|\psi_D H\rangle$, $|\psi'_D V\rangle$ are independently prepared regardless of the specific photon spatial mode (e.g., transversal electric magnetic mode like Hermite-Gaussian mode or Laguerre-Gaussian mode). The sLOCC measurements are implemented by single-photon detectors (SPDs) placed on L and R for single-particle counting (sLO) and by a coincidence device (CD), which deals with the electrical signals of SPDs and the trigger signals outputting coincidence counting on L and R, for classical communication (CC). An interference filter, whose full width at half maximum is 1 nm, and a single mode fiber (both not shown here) are placed before each SPD. A unit of polarization analysis detection (PAD), made of a quarter-wave plate (QWP), a HWP and a PBS (see inset of Fig. 2A), is locally employed to verify the predicted polarization entanglement by tomographic measurements and Bell test.

The setup generates from $|\Psi_{\text{prep}}\rangle$ by sLOCC the distributed resource state $|\Psi_{\text{LR}}\rangle$ of Eq. (2), with $\eta = 1$ (bosons), $l = \cos\alpha$, $r = \sin\alpha$, $l' = \sin\beta$ and $r' = \cos\beta$. This polarization entanglement is revealed in coincidence post-selection as in a common type of polarization-entangled photon source [31]. However, its origin is fundamentally different, arising from independently-prepared photons which do not share any common past but only need to meet at detectors. This entanglement is zero when the two spatial distributions remain separated each in a local region, being $\mathcal{I} = 0$ since the photons are distinguished by their locations (see section D in SM). We verify the entanglement versus $\mathcal{I}$ by adjusting different spatial distributions $|\psi_D\rangle$, $|\psi'_D\rangle$. To this aim we fix $\alpha = \pi/4$, implying $|\psi_D\rangle = (|\psi_L\rangle + |\psi_R\rangle)/\sqrt{2}$ and

$$|\Psi_{\text{LR}}\rangle = \cos\beta\ |\text{L}H, \text{R}V\rangle + \sin\beta\ |\text{L}V, \text{R}H\rangle\,, \qquad \textbf{(3)}$$

whose concurrence quantifying entanglement [6] is $C(\Psi_{\text{LR}}) = \sin 2\beta$, while $\mathcal{I} = -\cos^2\beta\ \log_2(\cos^2\beta) - \sin^2\beta\ \log_2(\sin^2\beta)$, as

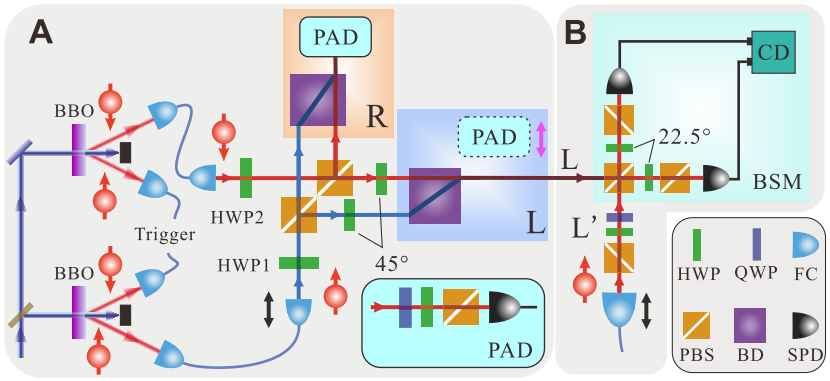

Fig. 2. Experimental setup. (A) Using fiber couplers (FCs), half-wave plates (HWPs) and polarized beam splitters (PBSs), two oppositely-polarized independent photons generated from two BBO crystals go to the separated regions L and R, where a beam displacer (BD) makes the photon paths meet at detectors. The inset displays the unit of polarization analysis detection (PAD), including a quarter-wave plate (QWP) and a single-photon detector (SPD). (B) Teleportation part. PAD is removed and the photons in L proceed to the Bell state measurement (BSM) with coincidence device (CD). The photon state to be teleported is generated in L′.

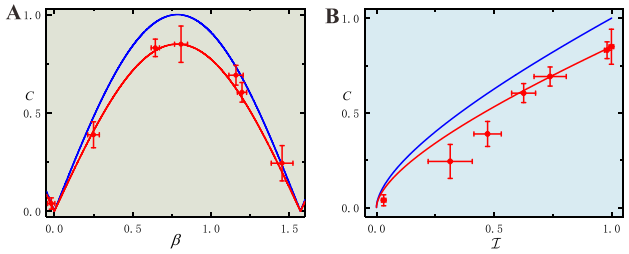

Fig. 3. Concurrence C for $\alpha = \pi/4$, versus β (A) and $\mathcal{I}$ (B). Blue (upper) curves are ideal theoretical predictions, red curves are the performance of the setup considering reduced visibility. Red dots (with error bars) are experimental results.

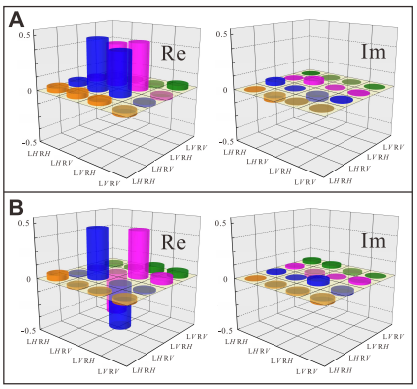

Fig. 4. Real and imaginary part of the reconstructed density matrix for $\alpha = \pi/4$ and: (A) $\beta = 0.808 \pm 0.041$ (expected state $|\Psi^+_{\rm LR}\rangle$); (B) $\beta = 2.406 \pm 0.040$ (expected state $|\Psi^-_{\rm LR}\rangle$).

obtained from Eq. (1), coincides with the entanglement of formation $E_f(\Psi_{\rm LR})$ of $|\Psi_{\rm LR}\rangle$ [24]. Thus, a monotonic relation $C = f(\mathcal{I})$ exists between concurrence and spatial indistinguishability. The experimental results of C, obtained after state reconstruction, versus both β and $\mathcal{I}$ are shown in Fig. 3A and B where the experimental points are lower than the ideal theoretical prediction due to the reduction of visibility while fit with the performance of this setup (see section C in SM). For $\beta = \pi/4$ ($\mathcal{I} = 1$), $|\Psi_{\rm LR}\rangle$ in Eq. 3 becomes the Bell state $|\Psi^+_{\rm LR}\rangle$. The generated state, in correspondence of $\beta = 0.808 \pm 0.041$, whose reconstructed density matrix is shown in Fig. 4A, has fidelity $(88.3 \pm 2.5)\%$ compared to $|\Psi^+_{\rm LR}\rangle$. We also perform the Bell inequality violation test ($S > 2$) [6] on this distributed resource state to directly prove the presence of nonlocal entanglement [32]. We experimentally achieve $S = 2.32 \pm 0.12$, violating the Bell inequality by about 2.7 standard deviations. Moreover, when $\beta = 3\pi/4$, that is when $|\psi'_{\rm D}\rangle = (|\psi'_{\rm L}\rangle - |\psi'_{\rm R}\rangle)/\sqrt{2}$ and $|\psi_{\rm D}\rangle$ are orthogonal yet completely spatially indistinguishable ($\mathcal{I} = 1$), the Bell state $|\Psi^-_{\rm LR}\rangle$ is expected. In the experiment, this state is created with fidelity $(88.3 \pm 2.4)\%$ for $\beta = 2.406 \pm 0.040$ (see Fig. 4B) and Bell inequality violation $S = 2.33 \pm 0.16$. These results prove that nonlocal entanglement is activated only by the remote spatial indistinguishability of independent photons.

Due to reduced visibility of the two heralded single photons, the experimental results that fit well with the performance of the employed setup are obviously lower than the theoretical prediction. Redoing the experiment with two photons from one BBO crystal, instead of two independent sources, allows us to obtain data closer to theory (see section E in SM).

Teleportation. We now show the indistinguishability-enabled entanglement is large enough to realize quantum teleportation. We can follow the standard protocol [6, 33] once the cases when both photons are either in L or in R are discarded. Following the above setup preparing the entangled state, the setup implementing teleportation is displayed in Fig. 2B. One of the two photons used as the trigger signals in Fig. 2A is sent to the side of L′ as the target to be teleported. The combination of a HWP and a QWP prepares the photon in a state $|\phi\rangle = a\,|H\rangle + b\,|V\rangle$ ($|a|^2 + |b|^2 = 1$). For teleporting the state $|\phi\rangle$ to the photon in R, we perform a Bell-state measurement (BSM) between L and L′, where the Bell state $|\Phi_{\rm LL'}\rangle = (|LH, L'H\rangle + |LV, L'V\rangle)/\sqrt{2}$ is measured by using a PBS and two HWPs at 22.5° [34, 35]. Correspondingly, the operation in R rotating its photon state to the desired one is $\sigma_x = |H\rangle\langle V| + |V\rangle\langle H|$, implemented by a 45° HWP. The signals from two SPDs are processed by a CD to coincide with the signals from R and triggers. Teleportation is achieved exploiting the distributed Bell state $|\Psi^+_{\rm LR}\rangle$, generated by $\mathcal{I} = 1$ of the original photons. We set $\alpha = \beta = \pi/4$ to maximize the generation proba-

state	$\|H\rangle$	$\|V\rangle$	$\|+\rangle$
$F_{\rm exp}$ (%)	90.4 ± 4.4	84.6 ± 5.9	78.7 ± 5.0
state	$\|-\rangle$	$\|\phi_-\rangle$	$\|\phi_+\rangle$
$F_{\rm exp}$ (%)	79.3 ± 4.9	93.2 ± 5.7	88.2 ± 5.4

Table 1. Fidelities of the six states $\rho_{\rm exp}$ with respect to the ideal state in the quantum teleportation process.

bility ($P_{\rm LR} = 50\%$). The six eigenvectors of σ_i ($i = x, y, z$) are the photon states in L′ to be teleported: $|\phi_{\rm ideal}\rangle \in \{|H\rangle, |V\rangle, |\pm\rangle = \frac{1}{\sqrt{2}}(|H\rangle \pm |V\rangle), |\phi_\pm\rangle = \frac{1}{\sqrt{2}}(|H\rangle \pm i|V\rangle)\}$. Performing quantum tomography of single-qubit state in R, the experimental teleported states $\rho_{\rm exp}$ are reconstructed based on four-photon coincidence. Fidelity $F_{\rm exp} = \langle\phi_{\rm ideal}|\rho_{\rm exp}|\phi_{\rm ideal}\rangle$ compared to the ideal state $\rho_{\rm ideal}$ is the figure of merit of teleportation efficiency. The measured fidelities, without background subtraction, are reported in Table 1, being higher than the classical fidelity limit of 2/3 [36]. The quantum process matrix χ of teleportation is reconstructed by comparing $\rho_{\rm ideal}$ and $\rho_{\rm exp}$ (see section D in SM), giving fidelity $F_\chi = (73.6 \pm 7.7)\%$. All error bars are estimated as standard deviation from the statistical variation of the photon counts, assumed to follow a Poisson distribution.

Discussion. We have designed a neat all-optical experiment generating nonlocal polarization entanglement by only adjusting the degree of remote spatial indistinguishability $\mathcal{I}$ of two initially-uncorrelated independent photons in two separated regions of measurement. This is basically different from swapping or heralded sources strategies, requiring initially entangled pairs. The value of $\mathcal{I}$ is tuned by controlling the spatial distribution of each photon wave packet towards the two operational regions. The photon paths only meet at the detection level. The setup implements the sLOCC [24] necessary to directly assess the relation between $\mathcal{I}$ and the amount of produced entanglement, verified by both state tomography and CHSH-Bell test. We remark that the sLOCC framework cannot produce any entanglement if the photons remain separated in the two regions, differently from optical interferometry with spread detection [37]. Notice that if the setup was run by two initially uncorrelated nonidentical particles, no entanglement would be obtained by measurements distinguishing particles from one another (LOCC). We have performed teleportation between the two operational regions, with fidelities (78-93%) above the classical threshold, by just tuning spatial indistinguishability of photons, with the advantage of not requiring inefficient or demanding entanglement source devices.

Our experiment fulfills an elementary entangling gate by bringing (uncorrelated independent) photons with opposite polarizations to the same local regions (nodes) and accessing the (nonlocal) entanglement by sLOCC measurements (see also a recent independent experiment [38]). So, entanglement activated by spatial indistinguishability is the product of both state structure and local measurements. Multiphoton entanglement can be produced by scalability of this elementary gate. The results open the way to viable indistinguishability-enhanced quantum information processing and quantum networking.

Funding. National Key Research and Development Program of China (2016YFA0302700, 2017YFA0304100); National Natural Science Foundation of China (11821404, 11774335, 61725504, 61805227, 61805228, 61975195, U19A2075); Anhui Initiative in Quantum Information Technologies (AHY020100, AHY060300); Key Research Program of Frontier Science, CAS (QYZDYSSW-SLH003); Science Foundation of the CAS (ZDRW-XH-2019-1); Fundamental Research Funds for the Central Universities (WK2030380015, WK2030380017, WK2470000026).

Disclosures. The authors declare no conflicts of interest.

REFERENCES

1. T. D. Ladd, F. Jelezko, R. Laflamme, Y. Nakamura, C. Monroe, and J. L. O'Brien, Nature **464**, 45 (2010).
2. H. Wang *et al.*, Phys. Rev. Lett. **123**, 250503 (2019).
3. F. Arute *et al.*, Nature **574**, 505 (2019).
4. A. D. Cronin, J. Schmiedmayer, and D. E. Pritchard, Rev. Mod. Phys. **81**, 1051 (2009).
5. D. Braun *et al.*, Rev. Mod. Phys. **90**, 035006 (2018).
6. R. Horodecki, P. Horodecki, M. Horodecki, and K. Horodecki, Rev. Mod. Phys. **81**, 865 (2009).
7. M. C. Tichy, F. Mintert, and A. Buchleitner, J. Phys. B: At. Mol. Opt. Phys. **44**, 192001 (2011).
8. G. Ghirardi and L. Marinatto, Phys. Rev. A **70**, 012109 (2004).
9. F. Benatti, R. Floreanini, and K. Titimbo, Open Syst. Inf. Dyn. **21**, 1440003 (2014).
10. H. M. Wiseman and J. A. Vaccaro, Phys. Rev. Lett. **91**, 097902 (2003).
11. P. Zanardi, Phys. Rev. A **65**, 042101 (2002).
12. A. P. Balachandran, T. R. Govindarajan, A. R. de Queiroz, and A. F. Reyes-Lega, Phys. Rev. Lett. **110**, 080503 (2013).
13. T. Sasaki, T. Ichikawa, and I. Tsutsui, Phys. Rev. A **83**, 012113 (2011).
14. F. Buscemi, P. Bordone, and A. Bertoni, Phys. Rev. A **75**, 032301 (2007).
15. S. Bose and D. Home, Phys. Rev. Lett. **110**, 140404 (2013).
16. N. Killoran, M. Cramer, and M. B. Plenio, Phys. Rev. Lett. **112**, 150501 (2014).
17. R. Lo Franco and G. Compagno, Sci. Rep. **6**, 20603 (2016).
18. S. Sciara, R. Lo Franco, and G. Compagno, Sci. Rep. **7**, 44675 (2017).
19. G. Compagno, A. Castellini, and R. Lo Franco, Phil. Trans. R. Soc. A **376**, 20170317 (2018).
20. S. Chin and J. Huh, Phys. Rev. A **99**, 052345 (2019).
21. N. Paunković, Y. Omar, S. Bose, and V. Vedral, Phys. Rev. Lett. **88**, 187903 (2002).
22. S. Bose, A. Ekert, Y. Omar, N. Paunković, and V. Vedral, Phys. Rev. A **68**, 052309 (2003).
23. A. Castellini, B. Bellomo, G. Compagno, and R. Lo Franco, Phys. Rev. A **99**, 062322 (2019).
24. R. Lo Franco and G. Compagno, Phys. Rev. Lett. **120**, 240403 (2018).
25. A. Castellini *et al.*, Phys. Rev. A **100**, 012308 (2019).
26. F. Nosrati, A. Castellini, G. Compagno, and R. Lo Franco, npj Quantum Inf. **6**, 39 (2020).
27. R. Hanbury Brown and R. Q. Twiss, Nature **178**, 1046 (1956).
28. T. Qureshi and U. Rizwan, Quanta **6**, 61 (2017).
29. S. Takeuchi, Opt. Lett. **26**, 843 (2001).
30. C. K. Hong, Z. Y. Ou, and L. Mandel, Phys. Rev. Lett. **59**, 2044 (1987).
31. C. E. Kuklewicz, M. Fiorentino, G. Messin, F. N. C. Wong, and J. H. Shapiro, Phys. Rev. A **69**, 013807 (2004).
32. F. Sciarrino, G. Vallone, A. Cabello, and P. Mataloni, Phys. Rev. A **83**, 032112 (2011).
33. D. Bouwmeester *et al.*, Nature **390**, 575 (1997).
34. N. Lütkenhaus, J. Calsamiglia, and K.-A. Suominen, Phys. Rev. A **59**, 3295 (1999).
35. J. Calsamiglia and N. Lutkenhaus, App. Phys. B **72**, 67 (2001).
36. S. Massar and S. Popescu, Phys. Rev. Lett. **74**, 1259 (1995).
37. D. Cavalcanti, M. França Santos, M. O. Terra Cunha, C. Lunkes, and V. Vedral, Phys. Rev. A **72**, 062307 (2005).
38. M. R. Barros, S. Chin, T. Pramanik, H.-T. Lim, Y.-W. Cho, J. Huh, and Y.-S. Kim, arXiv:1912.04208 [quant-ph] (2019).